Electronic Supplementary Material (ESI) for Analyst.

Electronic Supporting Information

In situ quantitative measurements on MMP-9 activity in single living cells by single molecule fluorescence correlation spectroscopy

Xintong Lu, Luoyu Ding, Haohan Song, Wenxin Yu, Chaoqing Dong*, Jicun Ren

School of Chemistry and Chemical Engineering, State Key Laboratory of Metal Matrix Composites, Shanghai Jiao Tong University, 800 Dongchuan Road, Shanghai 200240, China

E-mail address: cqdong@sjtu.edu.cn

Table of Contents

FCS Apparatus. The system was based on an inverted microscope (IX71, Olympus Optical Co., Japan). A 488 nm laser (Coherent, USA) and a 561 nm laser (Coherent, USA) were coupled into a single mode fiber and the output laser beam was employed as the excitation sources after the laser alignment. To avoid dye photobleaching and autofluorescence interference, the laser intensity was set at 45 μW. The intensity was controlled with neutral density attenuator. The laser beam was reflected by the dichroic mirror (ZT405/488/561/640, Chroma, USA) into the objective lens (60×NA 1.2, Olympus, Japan), where it was then focused on the sample solution on the cover glass. The fluorescence signals generated by the excitation of the sample were collected by the same objective, and divided into two detection channels via a dichroic mirror (540DRLP, Omega Optical, USA) and two emission filters (530DF30/590DF35, Omega Optical, USA). Finally, the signal passed through the pinhole in the front of single photon counter (SPCM-AQR16, PerkinElmer EG&G, Canada) and detected by SPCM. The generated signal fluctuations were real time collected and correlated in a digital correlator (Flex03lq12, Correlator.com, China). The obtained FCS raw curves were nonlinearly fitted with the Origin 8.0 software.

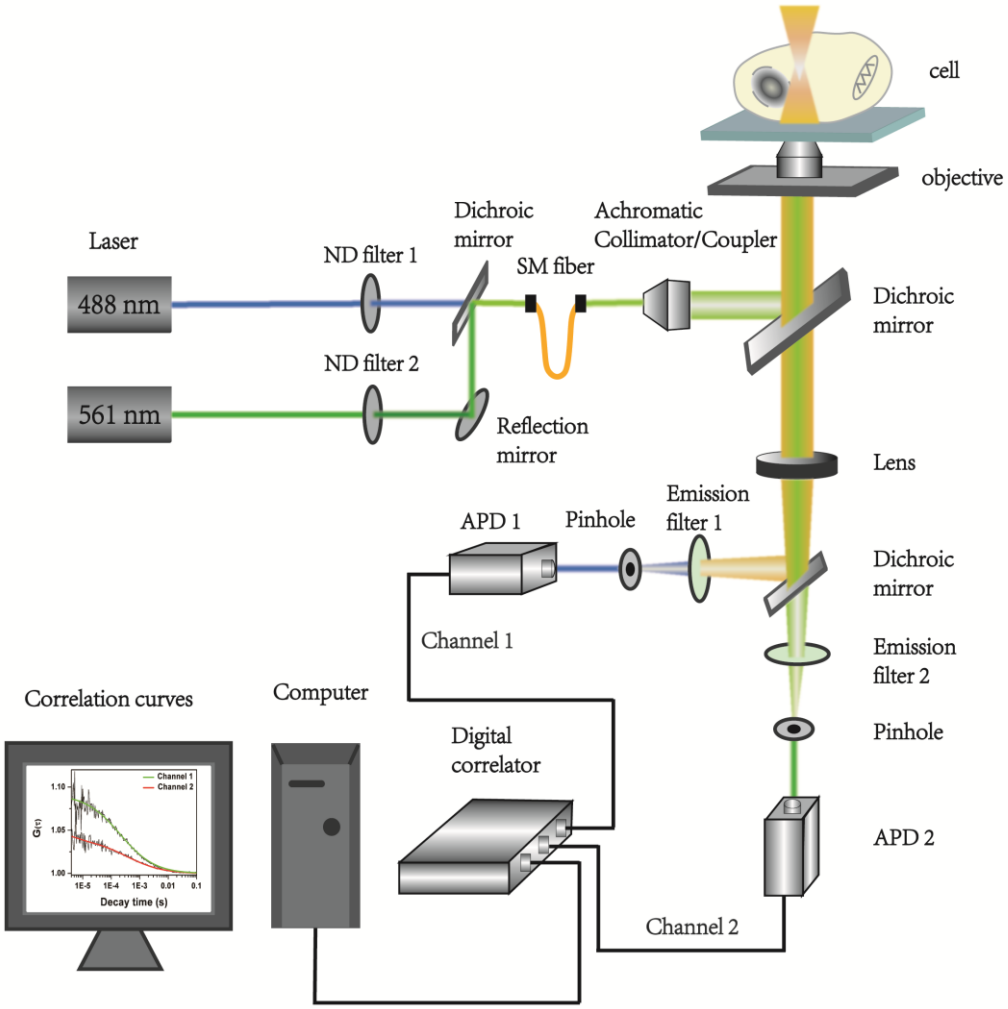

Figure S1. Schematic diagram of FCS system with two excitation and detection channels.

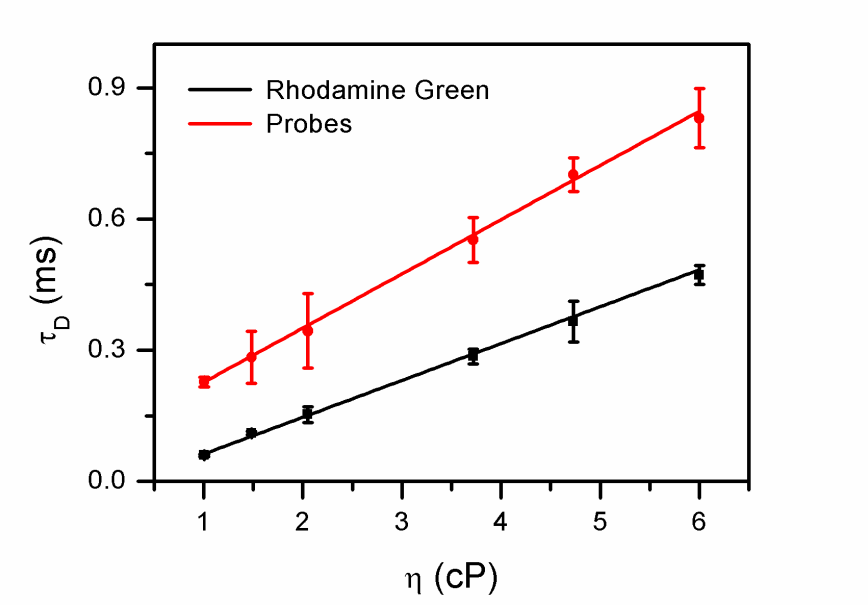

Figure S2. The effect of viscosity on the τ_D value of RG and probes.

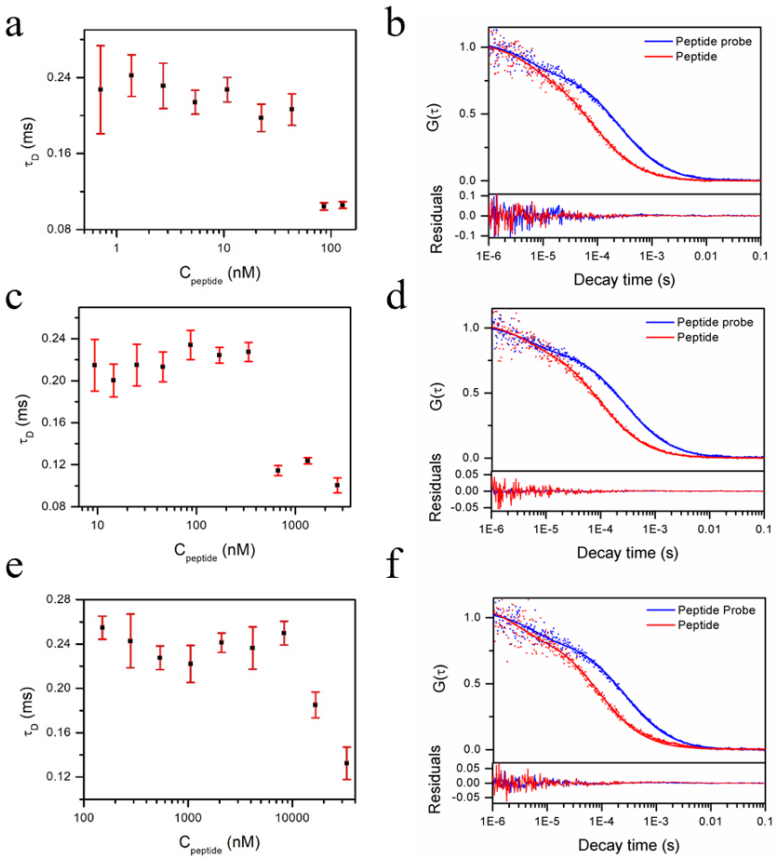

Figure S3. The influence of peptide concentration on the preparation of peptide probe. The dependence of τ_D values on the peptide concentration when different streptavidin concentrations were used (left) and the normalized autocorrelation curves of peptide probes and peptides (right). The concentration is 50 nM (a,b), 200 nM (c,d) and 1000 nM (e,f).

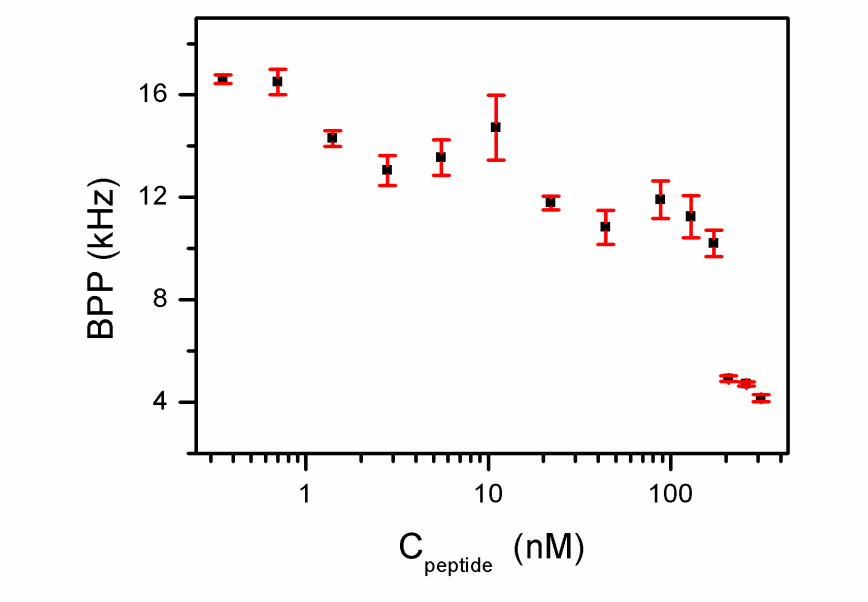

Figure S4. The influence of peptide concentration on BPP of peptide probe. Streptavidin concentration was fixed as 50.0 nM.

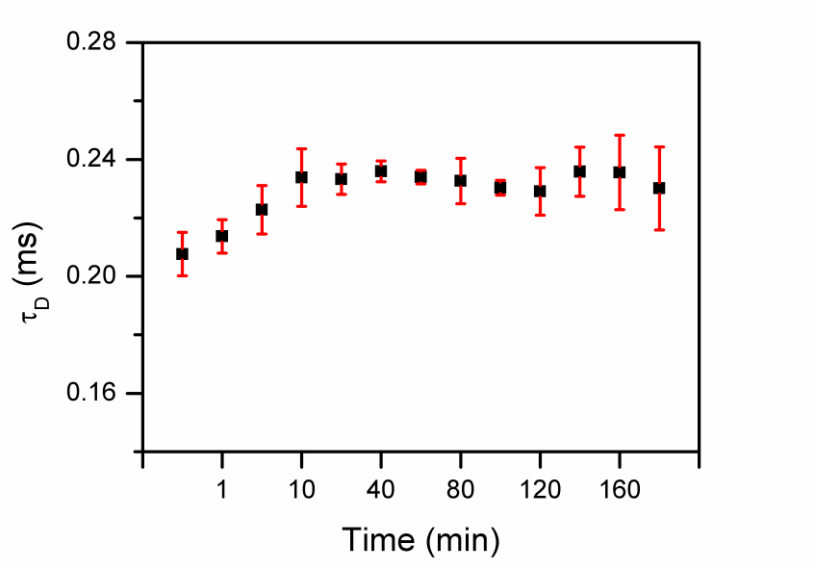

Figure S5. The influence of reaction time on the diffusion time of the prepared peptide probe.

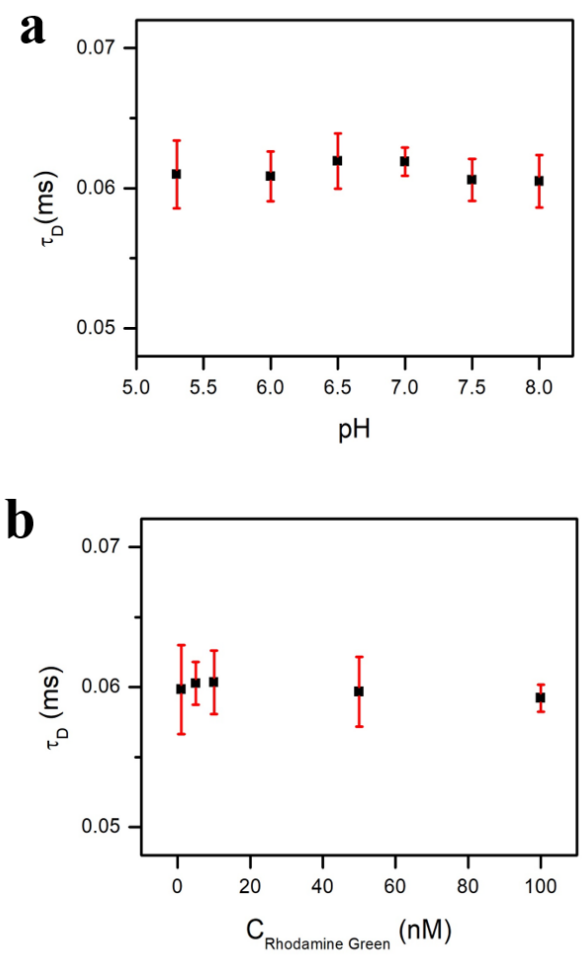

Figure S6. The influence of pH (a) and RG concentration on its diffusion time (b).

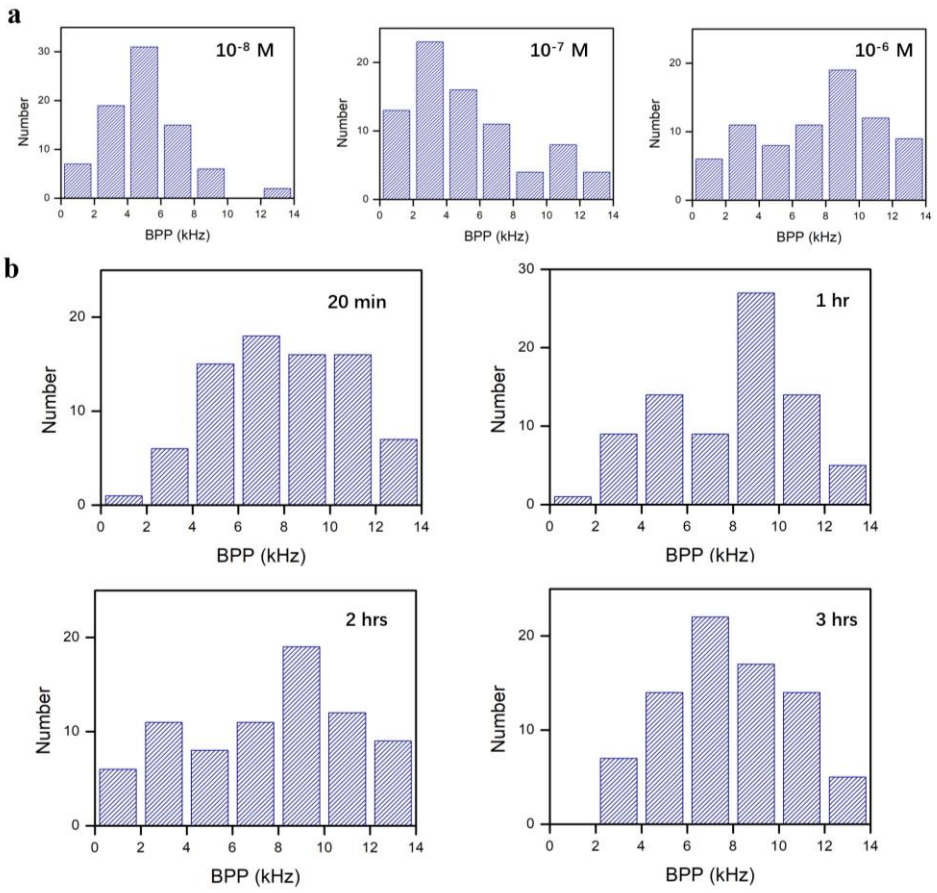

Figure S7. The influence of RG concentration and its incubation time on the BPP distribution of RG in single living cells. (a) HeLa cells were incubated with different concentrations of RG (10 nM, 100 nM, and 1000 nM); (b) HeLa cells were incubated with RG with different incubation times. (n = 80 cells each)

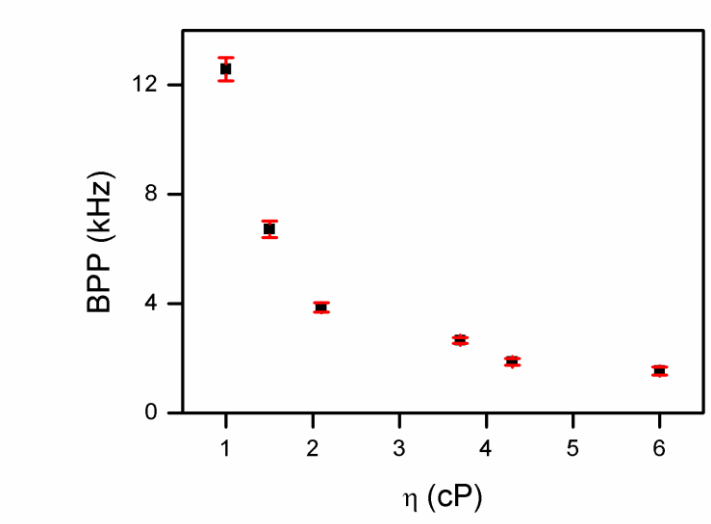

Figure S8. The effect of viscosity on brightness of BPP values of RG.

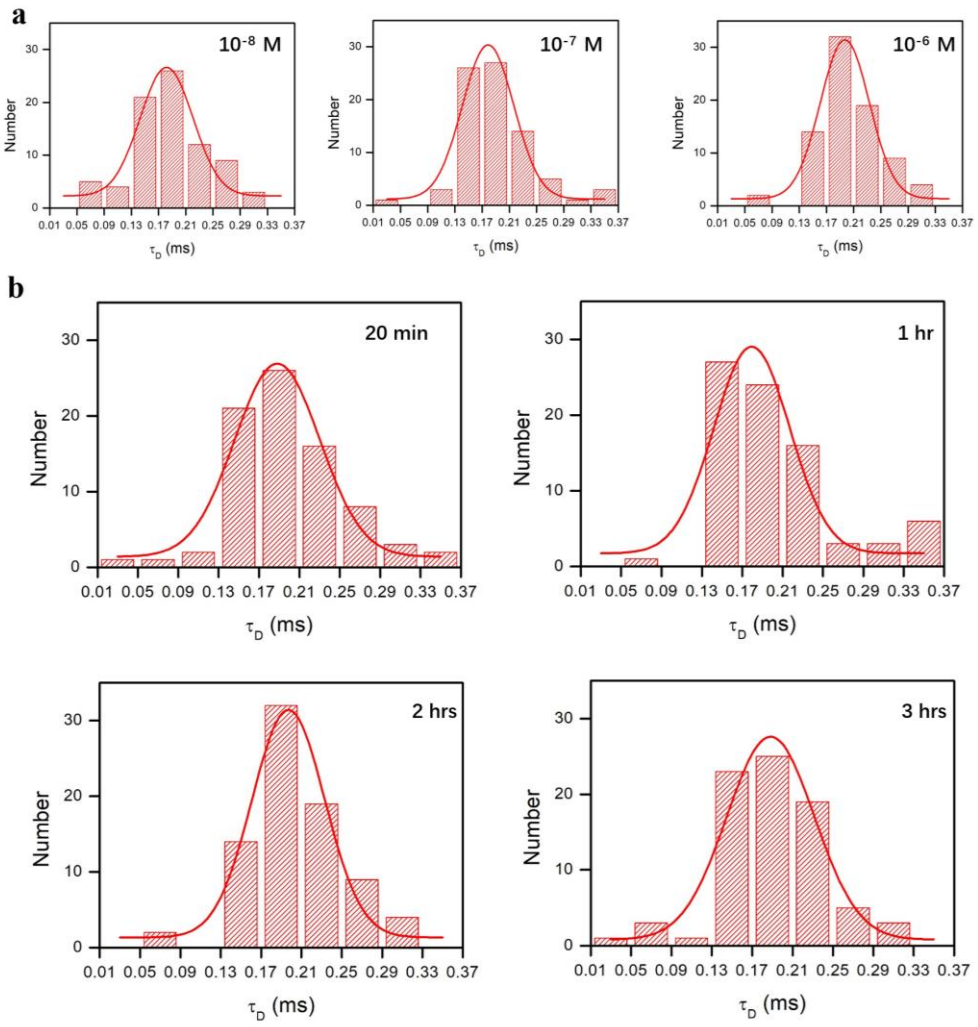

Figure S9. The influence of RG concentration and incubation time on the τ_D distribution of RG in single living cells. (a) HeLa cells were incubated with different concentrations of RG (10 nM, 100 nM, and 1000 nM); (b) HeLa cells were incubated with RG with different incubation times. (n = 80 cells each)

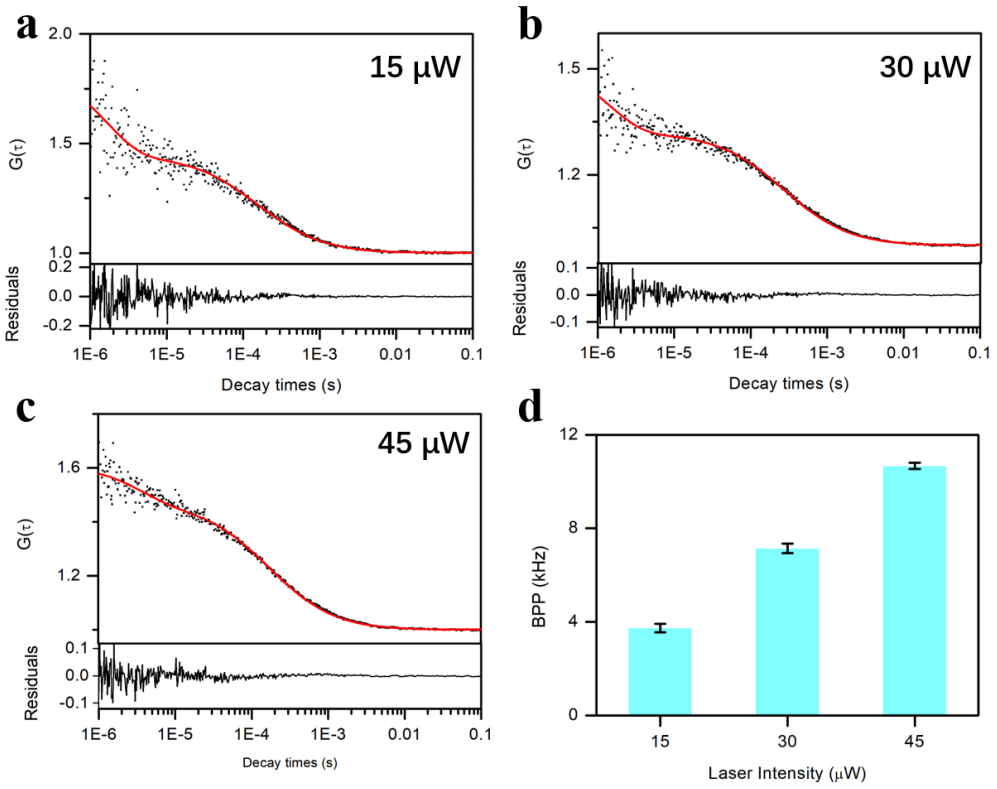

Figure S10. The influence of laser intensity. The autocorrelation curve of probe (a-c) and comparison of the determined BPP values (d). Laser intensity is 15 μW (a), 30 μW (b), and 45 μW (c).

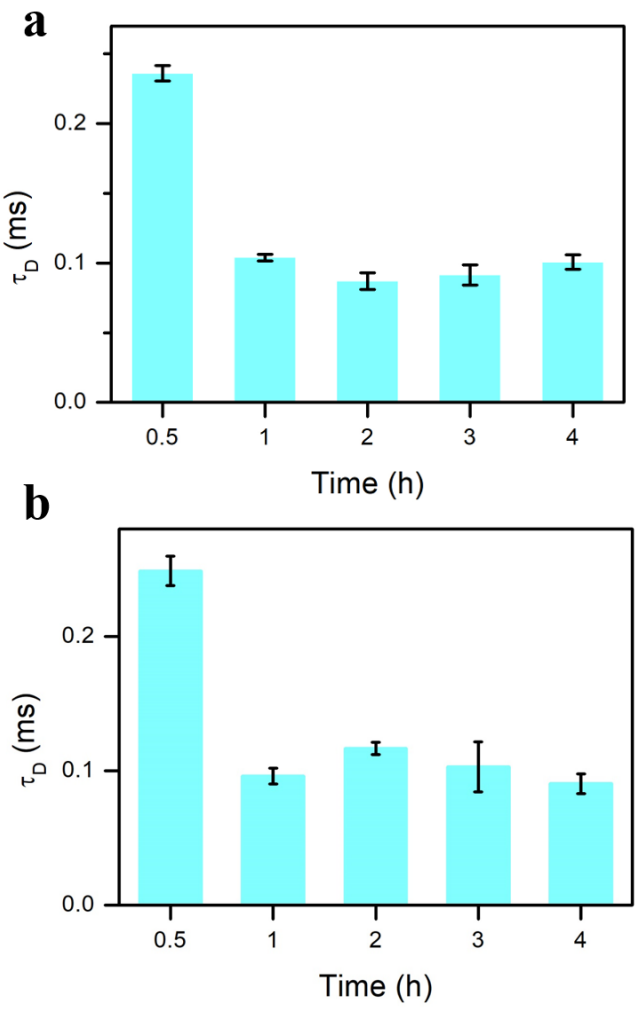

Figure S11. The influence of reaction time of MMP-9 on the diffusion time of probe. (a) In solutions; (b) In cell lysates.

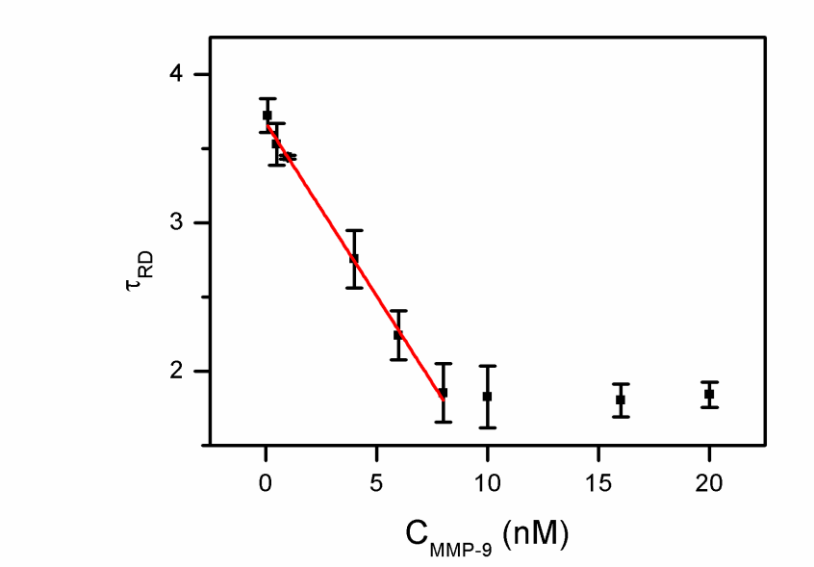

Figure S12. The linear relationship between τ_{RD} of reaction product and MMP-9 activity.

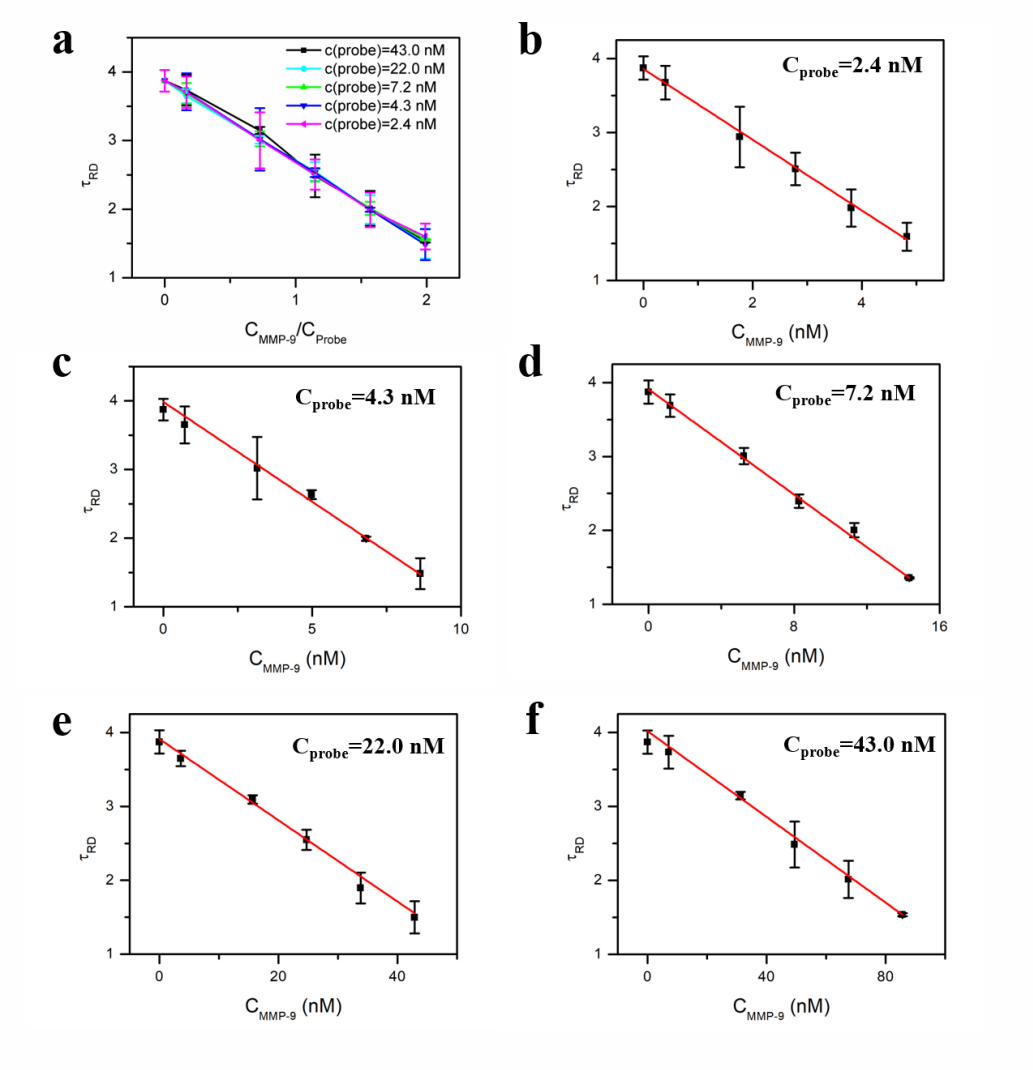

Figure S13. The different standard curves at different concentrations of probe. (a) Linear relations between the τ_{RD} values and the concentration ratio of MMP-9 to probes using different concentrations of probes. (b-f) Linear relation between τ_{RD} value and MMP-9 activity when 2.4 nM (b), 4.3 nM (c), 7.2 nM (d), 22.0 nM (e) and 43.0 nM (f) probes were used.

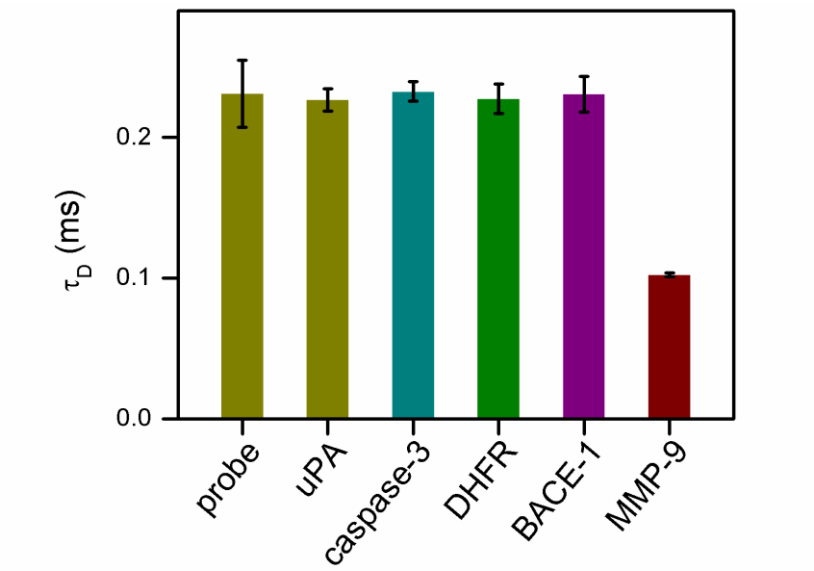

Figure S14. Selectivity of the assay. uPA (100 nM), caspase-3 (100 nM), DHFR (100 nM), and BACE-1 (100 nM) and MMP-9 (10 nM). Error bar represents the standard deviation (n = 3).

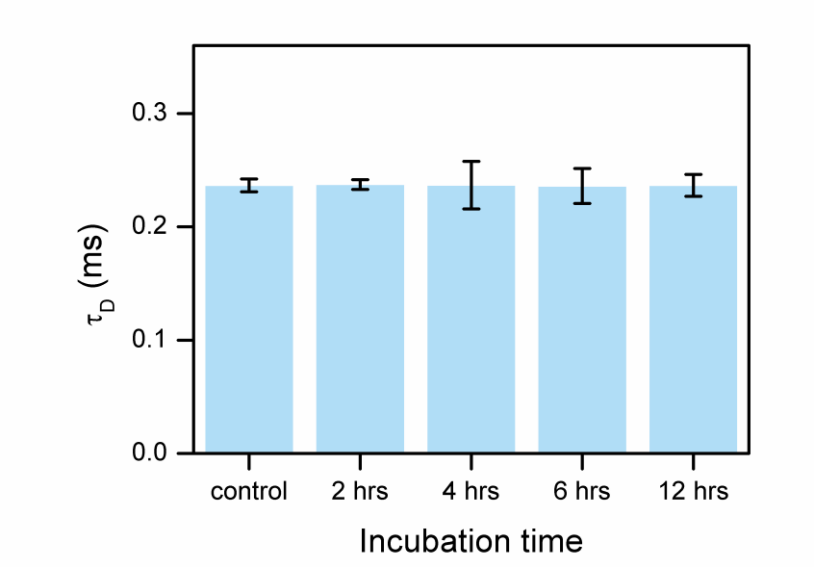

Figure S15. The τ_D change of probes with incubation times in the medium.

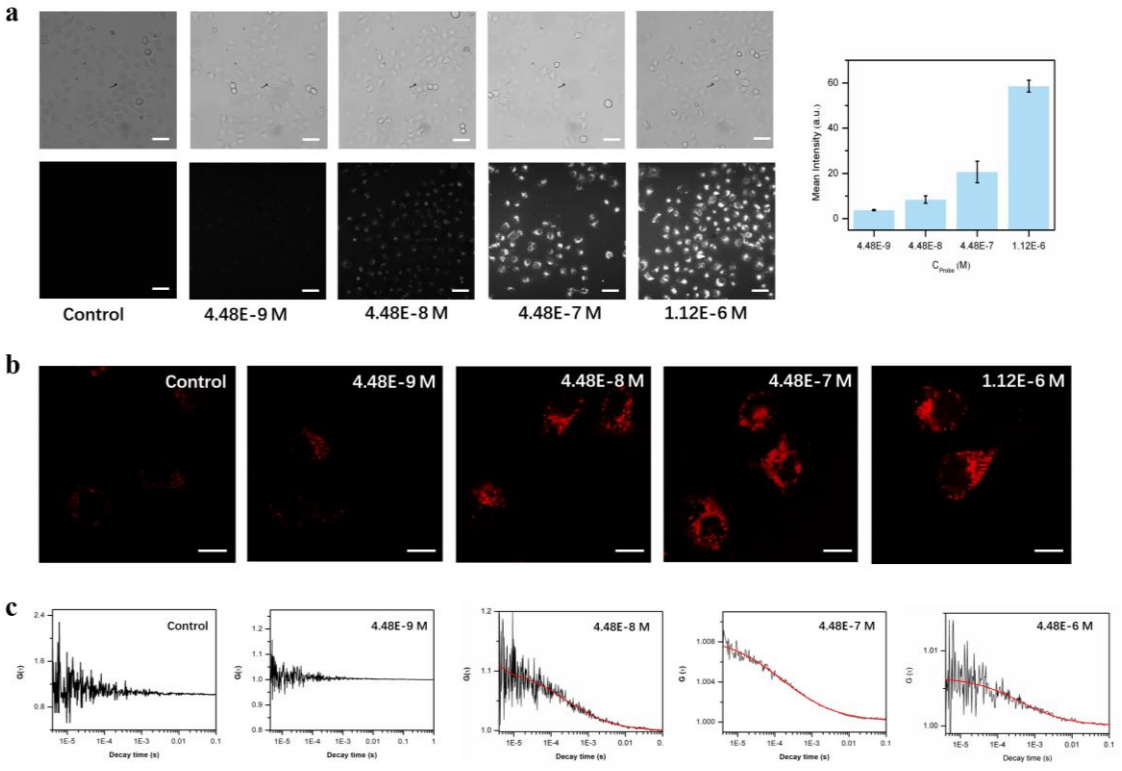

Figure S16. The influence of probe concentration on the PL intensity of cells and intracellular FCS curves. The incubation time is 2 hrs. (a) Bright field (upper) and fluorescence images (bottom) of HeLa cells with the RG concentration from 4.5 nM to 1.1 μM, the determined PL intensity of cell increased with probe concentrations(right). Its scale bar is 50 μm; (b)Typical confocal fluorescence microscopy images of cells. Its scale bar is 10 μm; (c) Typical FCS curves determined within the living cell.

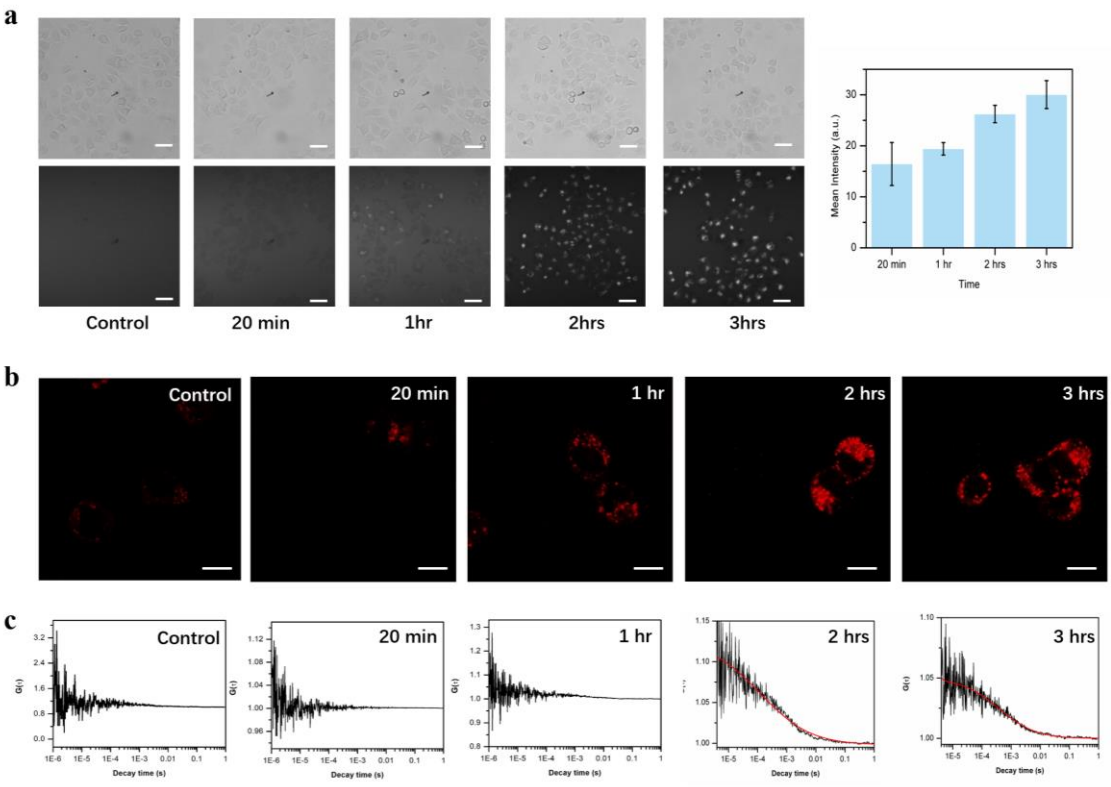

Figure S17. The influence of incubation time on *in situ* assay. The probe concentration was 44.8 nM. (a) Bright field (upper), fluorescence images (bottom) of HeLa cells**,** and its dependence of the determined PL intensity of cells on incubation time(right). Scale bar is 50 μm; (b) Typical confocal microscopy fluorescence images of cells**.** Scale bar is 10 μm; (c) Typical FCS curves determined within the living cell.

Table S1. Recovery of MMP-9 in cell lysates

C_{MMP-9} found (nM)	Added (nM)	Measured (nM)	Recovery (%)
	0.1	0.1	100.0%
	0.5	0.5	100.0%
	1.0	1.1	110.0%
2.5	2.0	2.0	100.0%
	3.0	2.9	96.7%
	4.0	4.2	105.0%
	5.0	5.0	100.0%

Table S2. Comparison of the determined IC_{50} values of different inhibitors with that by other methods or the known K_i values[1-4]

Inhibitors	IC_{50} (nM)	Known IC_{50} (nM)	Known K_i (nM)
GM6001	23.3	0.5	0.57
Marimastat	40.7	3	---
Actinonin	193.9	---	330

Table S3. Comparison of the reported methods for MMP-9[5-10]

Assay system	Linear ranges	LOD	Real samples	Ref.
Colorimetry	16 pg mL^{-1}~100 ng mL^{-1}	11 pg mL^{-1}	plasma	[5]
Luminescent biosensor	5 pM~0.25 nM	2.1 pM	MCF-7 cells (extracellular secretion)	[6]
Electrochemical biosensor	0.01 nM -90 nM	10 pM	Spiked Urine Samples	[7]
Fluorescence assay using nanofiber substrate	0-100 pM	10 pM	cocktail solutions	[8]
Fluorescence assay using peptide microarray	50 pg mL^{-1}~100 ng mL^{-1}	60 pg mL^{-1}	MDA-MB-231 cells (extracellular secretion)	[9]
FRET	N.A.	0.74 nM	mouse models (in vivo)	[10]
FCS	0.2 nM-8 nM	0.1 nM	Hela cells (in vivo)	this study

Notes and References

(1) Akter, H.; Park, M.; Kwon, O. S.; Song, E. J.; Park, W. S.; Kang, M. J. Activation of matrix metalloproteinase-9 (MMP-9) by neurotensin promotes cell invasion and migration through ERK pathway in gastric cancer. *Tumor Biol.* **2015**, *36*, 6053-6062.

(2) Wahl, R. C.; Pulvino, T. A.; Mathiowetz, A. M.; Ghose, A. K.; Johnson, J. S.; Delecki, D.; Cook, E. R.; Gainor, J. A.; Gowravaram, M. R.; Tomczuk, B. E. Hydroxamate inhibitors of human gelatinase B (92 kDa). *Bioorg. Med. Chem. Lett.* **1995**, *5*, 349-352.

(3) Mondal, S.; Adhikari, N.; Banerjee, S.; Amin, S. A.; Jha, T. Matrix metalloproteinase-9 (MMP-9) and its inhibitors in cancer: A minireview. *Eur. J. Med. Chem.* **2020**, *194*, 112260.

(4) Whittaker, M.; Floyd, C. D.; Brown, P.; Gearing, A. J. H. Design and therapeutic application of matrix metalloproteinase inhibitors *Chem. Rev.* **2001**, *101*, 2205-2205.

(5) Ruiz-Vega, G.; Garcia-Robaina, A.; Ben Ismail, M.; Pasamar, H.; Garcia-Berrocoso, T.; Montaner, J.; Zourob, M.; Othmane, A.; del Campo, F. J.; Baldrich, E. Detection of plasma MMP-9 within minutes. Unveiling some of the clues to develop fast and simple electrochemical magneto-immunosensors. *Biosens. Bioelectron.* **2018**, *115*, 45-52.

(6) Su, H. J.; Zang, M. H.; Lu, L. H.; Li, F. Monitoring matrix metalloproteases based on the selective interaction between an Ir(iii) solvent complex and a histidine-rich polypeptide. *Chem. Commun.* **2019**, *55*, 7085-7088.

(7) Guo, B. Y.; Song, P.; Zhou, K.; Liu, L.; Wu, H. C. Simultaneous Sensing of Multiple Cancer Biomarkers by a Single DNA Nanoprobe in a Nanopore. *Anal. Chem.* **2020**, *92*, 9405-9411.

(8) Han, S. W.; Koh, W. G. Hydrogel-Framed Nanofiber Matrix Integrated with a Microfluidic Device for Fluorescence Detection of Matrix Metalloproteinases-9. *Anal. Chem.* **2016**, *88*, 6247-6253.

(9) Lei, Z.; Gao, J. X.; Liu, X.; Liu, D. J.; Wang, Z. X. Peptide microarray-based fluorescence assay for simultaneously detecting matrix metalloproteinases. *Anal. Methods*, **2016**, *8*, 72-77.

(10) Ma, T. C.; Hou, Y.; Zeng, J. F.; Liu, C. Y.; Zhang, P. S.; Jing, L. H.; Shangguan, D.; Gao, M. Y. Dual-Ratiometric Target-Triggered Fluorescent Probe for Simultaneous Quantitative Visualization of Tumor Microenvironment Protease Activity and pH in Vivo. *J. Am. Chem. Soc.* **2018**, *140*, 211-218.